Revista Mexicana de Física **43**, *No. 4 (1997) 622–633*

Experimental techniques in heavy ion fusion II. particle technique

E.F. AGUILERA AND J.J. VEGA
Departamento de Aceleradores
Instituto Nacional de Investigaciones Nucleares
Apartado postal 18-1027, C.P. 11801, Mexico, D.F.

J.J. KOLATA
Physics Department, University of Notre Dame
Notre Dame, Indiana 46556, USA

Recibido el 19 de febrero de 1997; aceptado el 4 de abril de 1997

ABSTRACT. An experimental technique in the field of heavy ion fusion, involving a recoil velocity spectrometer designed to detect the evaporation residues in fusion reactions, is described in detail. Monte Carlo calculations are performed which allow the determination of the main features of the spectrometer. Some representative experimental results are presented and a comparison is made with the results of other works using independent methods. Finally, a global comparison is made of this technique with the gamma-ray technique described previously in the first part of this work.

RESUMEN. Se describe en detalle una técnica experimental en el campo de la fusión con iones pesados, la cual involucra un espectrómetro de velocidades de retroceso diseñado para detectar los residuos de evaporación en reacciones de fusión. Se efectúan cálculos de Monte Carlo que permiten la determinación de las principales características del espectrómetro. Se presentan algunos resultados experimentales representativos y se hace una comparación con los resultados de otros trabajos que usan métodos independientes. Finalmente, se hace una comparación global de esta técnica con la técnica de rayos gamma descrita previamente en la primera parte de este trabajo.

PACS: 29.30Cm; 25.70.Jj

1. INTRODUCTION

The study of fusion reactions induced by heavy ions has become an important tool for understanding the processes occurring in the interaction between nuclei. Interest in this field was much increased in the middle eighties by the observation that many systems exhibit sub-barrier fusion cross sections which are considerably enhanced with respect to expectations based on simple one-dimensional barrier penetration models. As is well known, these models succesfully describe most above-barrier data.

For systems which are not too heavy, at not too high energies, the dominant decay mode of the corresponding compound nucleus is particle evaporation. The complete

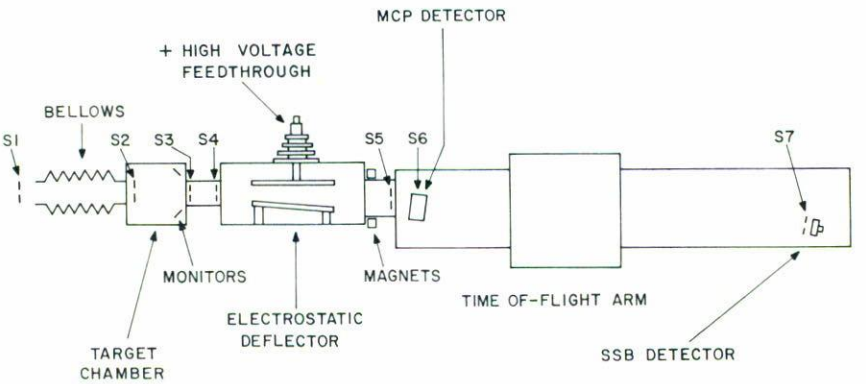

FIGURE 1. Schematic side view of the spectrometer. S1, ..., S7 are the slits referred to in the text.

fusion cross sections can then be experimentally determined by measuring the corresponding evaporation residues (ER). The γ-ray technique, which was thoroughly discussed in a previous paper [1], provides in principle an indirect method of measuring said ER. However, for the low cross sections involved in sub-barrier fusion, the corresponding peak-to-background ratios in the γ-ray spectra become unmeasurably small thus producing serious inconveniences in the method. Direct measurement of the residues using particle detection techniques is then the best choice. The major difficulty in detecting the ER comes from the fact that their angular distribution is always forward peaked, so that they are normally embedded in a background of about 10^9 beam particles per second. It is thus necessary to reduce the intensity of the transmitted beam to a manageable counting rate and to identify the ER, separating them from the residual beam-like particles which still reach the detection system.

These objectives can be achieved by means of an electrostatic deflector operating in combination with a time-of-flight/energy telescope. The fact that beam and ER have in general different electrostatic rigidities (energy/charge) allows one to separate them out by the transverse electric field produced in the deflector. The measurement of time (or velocity) and energy, on the other hand, allows for mass identification.

In this paper we report on a recoil velocity spectrometer designed to detect ER, whose operation is based on the two-step procedure above mentioned. The spectrometer is described in detail in Secttion 2. Monte Carlo calculations performed to determine the main features of the spectrometer are described in Sect. 3. In Section 4, representative results of some experiments performed with the spectrometer are presented and a comparison with some previous works using independent methods is made. Finally, in Section 5, we present the conclusions of this work.

2. DESCRIPTION OF THE SPECTROMETER

A schematic view of the spectrometer is shown in Fig. 1. The electrostatic deflector (ED), placed at about 30 cm from the target, consists of two mirror-polished stainless steel plates, with rounded edges, which are contained in a rectangular box. The upper

TABLE I. Positions and radii of the slits S1, ..., S7 of Fig. 1. The chosen coordinate system has origin on the target center with y-axis pointing downwards and z-axis pointing to the right in Fig. 1.

Slit	y(cm)	z(cm)	R(mm)
1	0.00	−26.07	0.15
2	0.00	− 1.00	0.23
3	0.00	13.18	0.33
4	0.00	22.97	0.36
5	1.93	70.43	0.30
6	2.44	78.38	0.89
7	8.89	178.38	0.95

plate is horizontal and electrically isolated so that a variable voltage can be applied to it through a high-voltage high-vacuum feedthrough. The lower plate is grounded and tilted 4° with respect to the horizontal plane to prevent the deflected ions exiting the deflector from hitting it. Typical fields of around 30 kV/cm, requiring no conditioning period, have been applied to the deflector during normal operation.

The time-of-flight (TOF) arm consists of two 8-inches pipes joined by an intermediate cubic box which supports a 1000 l/s cryogenic pump. A microchannel-plate detector (MCP) placed at the entrance of the arm provides a time signal by measuring the secondary electrons produced by the passage of the ions through a 10 μg/cm^2 carbon foil. A second time signal as well as an energy signal are provided by a 400 mm^2 silicon surface barrier detector (SSB) placed at the rear end of the TOF arm, at approximately 1 m from the MCP. This detector is mounted in a special frame which allows for three degrees of freedom so that the detector can be moved back and forth along the pipe, it can be moved up and down in the vertical direction, and it can be tilted so as to face perpendicularly the incoming particles.

The ED and TOF arm are rigidly coupled to the target chamber, which is a cubic box mounted on a rotating bearing and coupled to the beam line through a flexible bellows. The whole system can thus be rotated in the horizontal plane around a fixed target so that angular distributions in the range of ±12° (determined by the bellows flexibility) can be measured. The target holder supports up to three targets which can be externally moved in and out the beam path without breaking the vacuum. Upstream the target chamber, another 1000 l/s cryogenic pump is used to pump down the system. Typical pressures of 6×10^{-7} torr are usually achieved during normal operation. Seven circular slits, indicated by S1, ..., S7 in Fig. 1, completely define the geometry of the system. In an effort to minimize slit scattering, slits 3, 4, 5 and 7 were made with thin Cu foil and finished with sharp inner edges. The exact positions and sizes of the slits are indicated in Table I. Slit 6 is actually the frame supporting the MCP carbon foil but it is included in Table I because its alignment is an important (but not critical) parameter in the spectrometer. Two permanent magnets placed upstream slit 5 serve to prevent the electrons knocked out from that slit by the beam from disturbing the performance of the ED.

A system of four SSB detectors placed symmetrically at an angle of 15° with respect to the nominal beam direction was used to normalize the data. In the usual method, where only one monitor is used (or the less usual one with two monitors), the fast variation of the Rutherford cross section at small angles makes the results strongly dependent on equipment-alignment and beam-focusing conditions. Five parameters must be simultaneously determined in principle in order to eliminate this dependence. These are related to the beam direction (θ,ϕ), the beam spot position on target (x, y), and the normalizing factor given by the product of the integrated charge times the target thickness (Qt). It can be shown [2], however, that three detectors suffice to deduce Qt with high precision provided the beam inclination is not too great ($\leq 4°$). By using 4 monitors, a very reliable estimation of the associated uncertainty can be additionally obtained. A typical precision of about 1% in the normalization factors for the differential cross sections has been obtained with our method, which is about 20 (4) times better than that of the 1 (2)-monitor method under reasonably good alignment conditions. A detailed description of our normalization method can be found in Ref. 2.

3. TRANSMISSION EFFICIENCY AND MONTE CARLO CALCULATIONS

The determination of the transmission efficiency plays a key role in the cross section measurements with this kind of apparatus. The fact that the evaporation residues that enter the electrostatic deflector within a given solid angle do actually have different charges and/or energies, effectively changes the solid angle defined by the deflected exiting particles. Any transmission determination must thus take into account this dynamic effect caused by the electrostatic deflector. From the geometry of our apparatus, (Fig. 1), it is clear that the slit at the entrance of the TOF arm, S5, defines the entrance solid angle (58 μsr) for the spectrometer. The transmission efficiency is thus defined as the ratio of the number of particles actually detected to those initially traveling (before being deflected) within this solid angle.

A Monte Carlo code was written in order to simulate the physical phenomena occurring in the spectrometer. An event here consists of a given residue leaving the target at a certain position, flying in a certain direction and having a specified energy and charge. The way to generate such an event, summarized in Table II, is the following: the fusion residues distribution must be given as an input to the code, and can be obtained from some of the existing statistical-evaporation codes such as CASCADE [3] or LILITA [4]. The position on target of the leaving residues, determined by its polar coordinates (r, φ), is generated by using a uniform distribution for φ $(0 \leq \varphi \leq 2\pi)$ and either a uniform or a Gaussian distribution for r, with parameters provided by the user according to the size of the beam spot on target. To generate the direction of flight of the residues, specified by the two angles (θ, ϕ), a uniform distribution is used for ϕ $(0 \leq \phi \leq 2\pi)$ while a Gaussian distribution, centered at the beam direction, is used for θ; the width of this Gaussian is usually taken from the measured angular distribution, if any, or else it can be estimated from momentum conservation and angular straggling considerations. Both the energy and the charge of the residues are also generated with Gaussian distributions. For the energy, the centroid is determined from the beam energy taking into account momentum

TABLE II. Event generation for the Monte Carlo calculations.

Generated parameters (description)	Distribution used
A, Z (residue)	From CASCADE [3] or LILITA [4]
r, φ (position on target)	r: uniform or gaussian, φ: uniform in $[0, 2\pi]$
θ, ϕ (flight direction)	θ: gaussian; $\overline{\theta} = \theta_{\rm beam}$; σ_θ from exp. ϕ uniform in $[0, 2\pi]$
$E_{\rm ER}$ (residue energy)	Gaussian, $\overline{E}_{\rm ER} = [A_{\rm ER} A_p/(A_p + A_t)^2](E_{\rm beam} - E_{\rm loss})$ σ_E from exp.
q (charge)	Gaussian, $\overline{q}$ and σ_q from Ref. 5

conservation and energy-loss, while the width can be given by some estimation taking into account the energy carried by the evaporated particles and the energy straggling in the target. Since this estimation is rather cumbersome to do, we usually considered the width as a free parameter which was varied until the width of the energy spectrum observed in the SSB detector was reproduced. The parameters for the charge distribution were taken from Ref. 5.

The history of every residue generated in this way is followed throughout the spectrometer until it stops either at one of the slits or at the SSB detector. In order to determine the path of the residues in the region of the electrostatic deflector, Laplace's equation was numerically solved in two dimensions with appropriate boundary conditions determined by the plates and the containing box. The transmission efficiency can thus be determined for any voltage applied to the deflector. Since experimentally the value of this voltage is selected so as to maximize the yield from each target, the same optimization is made in the code in order to determine the predicted transmission efficiency. Fortunately, it was found both experimentally and theoretically that the dependence of the transmission on the deflector voltage is weak, the transmission being stable against $\pm 5\%$ deviations in the applied voltage.

In practice, the transmission efficiency of the spectrometer for given ER (given reaction) is determined empirically by elastic scattering of ions of similar atomic and mass numbers, and kinetic energy. So, for example, for experiments where the Al+Ge [6], the Cl+Ni [7], the S+Ni [8], or the O+Ge [9] systems were measured, the transmission efficiency was determined by measuring the Rutherford scattering of ^{103}Rh and/or ^{81}Br beams on a ^{60}Ni target at selected energies, while the elastic scattering of ^{58}Ni on ^{24,26}Mg was measured at an appropriate energy in order to determine the corresponding efficiency for an experiment on some Si+Mg systems [10]. For O+C systems, on the other hand, the transmission was measured by elastically scattering a ^{28}Si beam from carbon targets [11].

The empirical and predicted values of the transmission efficiency for residues in the region of $A \sim 90$ are presented as a function of their outgoing energy in Fig. 2, where filled symbols refer to experimental values while open symbols correspond to Monte Carlo calculations. By looking first at the theoretical predictions, we note the following important features: (a) There is no appreciable energy dependence of the transmission

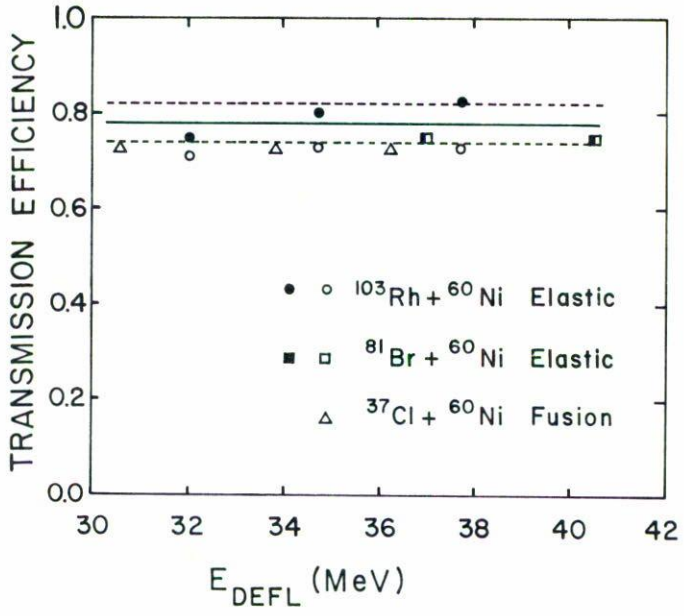

FIGURE 2. Transmission efficiency as a function of the residue outgoing energy. Filled symbols refer to experimental values while open symbols correspond to Monte Carlo calculations.

efficiency for the given energy range. (b) Calculations for elastically scattered particles give essentially the same values as those for actual fusion residues, which justifies the mentioned approach to experimentally determine the efficiency. (c) Efficiency variation with mass is also negligible for the involved mass region, as indicated by the calculations with Rh and Br beams.

It is thus reasonable to use one single value for the transmission efficiency of the spectrometer in the specified energy and mass ranges, and to take this value as the average of the five experimental points, $T = 0.780 \pm 0.045$. This value and its error are indicated by the solid and dashed lines, respectively, in Fig. 2. Taking into account the nature of the calculations, the agreement of the theoretical and experimental values is considered good, and this value of the transmission has been used in the normalization of several data sets [6–8]. A similar situation was encountered for residues in the region of A about 50 with E around 20 MeV, for which the measured transmission efficiency, obtained by scattering Ni from Mg, was $T = 0.70 \pm 0.04$, which is also in good agreement with the corresponding Monte Carlo calculation. Additional results used for the fusion of O+C at lab energies between 14.5 and 25 MeV (residues of around 11 MeV), which were obtained by scattering ^{28}Si from C, indicated that the transmission through the electrostatic deflector is energy dependent for these lighter compound systems, ranging from about 50% to 70% at the lowest and highest energies, respectively [11]. A quadratic function of energy was used to fit the transmission in this case, in good agreement with the respective Monte Carlo results. An energy dependence for the transmission was also found for the slow ER resulting from the fusion of O+Ge at laboratory energies in the region from 38 to 66 MeV, measured by scattering ^{81}Br ions on ^{70}Ge. In this case the

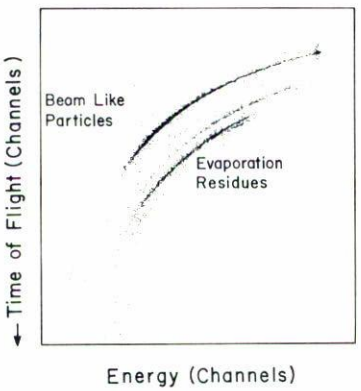

FIGURE 3. Two-dimensional plot of time of flight (TOF) *versus* energy for the $^{17}O+^{12}C$ system at $\theta = 5°$ and a ^{17}O beam energy of 25 MeV.

transmission probability ranged from about 49% at the lowest energies to 56% at the highest energies, following a nearly linear behavior [9]. The corresponding Monte Carlo calculations gave again consistent results.

4. TYPICAL EXPERIMENTAL RESULTS

A typical example of the raw data obtained with this spectrometer is shown in Fig. 3. This TOF versus energy plot was taken for the $^{17}O+^{12}C$ system at $\theta = 5°$ and ^{17}O beam energy of 25 MeV. The beamlike particles, with a large range of energies, are clearly distinguishable from the ER of interest. The mass parabolas in this figure can be projected onto the mass axis to obtain the mass spectrum shown in Fig. 4. The centroids for the various peaks are indicated there, together with the corresponding FWHM values (given in parentheses). A mass resolution $\Delta m/m$ better than 0.05 can be assigned to the spectrometer on the basis of this figure.

The mass 24 group, appearing in Figs. 3 and 4 between the beam-like particles and the main ER group, may result from a pickup of two alphas followed by a single neutron decay $(2\alpha, n)$ or from the formation of a compound nucleus followed by the emission of an alpha particle and a neutron (αn). By looking at the velocity spectra for this mass group, the two components can be properly separated [11]. The main consideration here is that the high energy end of the group corresponds to the direct reaction channel events, while those events with energies similar to the strong ER group are the fusion events. Similarly, the strong group at the high energy tip of the beamlike mass parabola in Fig. 3 results from true $(\theta_{lab} = 5°)$ elastically scattered ^{17}O ions.

Once the problem of positively identifying the ER has been solved, the corresponding angular distributions can be determined to obtain the total fusion yield. Some typical angular distributions are presented in Fig. 5 for the $^{16}O + {}^{70,72,73,74,76}Ge$ systems. Even though the targets used for the several systems in this figure had widely varying thicknesses (the ^{72}Ge target was about a factor of 5 thicker than the ^{74}Ge target and a factor of 2 thicker than the ^{70}Ge target), it can be shown [9] that the similar widths reported in

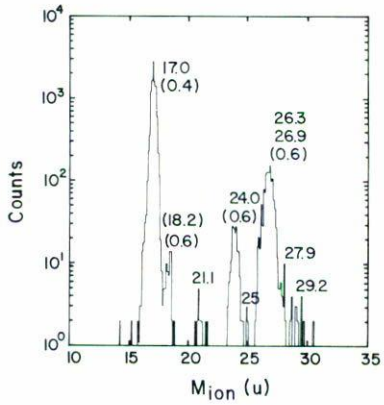

FIGURE 4. Projection of Fig. 3 onto the mass axis. The centroids and FWHM values (in parentheses) are indicated here. The two centroids at 26.3 and 26.9 are the result of a double Gaussian fit to the peak, where the widths were forced to be 0.6.

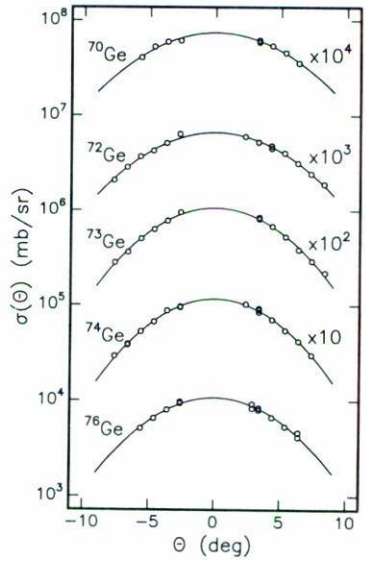

FIGURE 5. Angular distributions obtained for ^{16}O + $^{70,72,73,74,76}Ge$ at E_{cm} = 40.3, 40.1, 40.8, 40.9, and 41.1 MeV, respectively. The error bars are smaller than the points in all cases. The widths (standard deviations) of the fitted Gaussians (solid lines) are 5.3°, 5.2°, 4.6°, 4.5°, and 4.7°, respectively.

the caption are consistent with the results of realistic estimations of multiple scattering in the target, the most important contribution to the widths coming from the kinematic spread of the residues. Since the distributions are symmetric about $\theta = 0°$, the measurement of both positive and negative angles allows for interpolation to the important region of small angles, determining at the same time the 0° position of the time-of-flight arm with high precision.

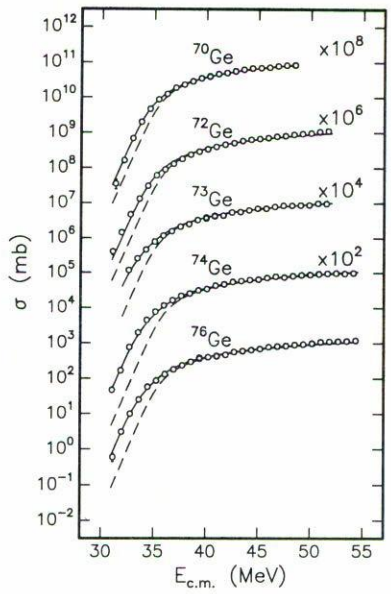

FIGURE 6. Experimental fusion cross sections obtained with the recoil velocity spectrometer for $^{16}O + {}^{70,72,73,74,76}Ge$. The dashed curves correspond to one-dimensional barrier penetration calculations, while the solid curves are the results of the best-model calculations obtained in Ref. 9.

Under the assumption that the angular distributions have nearly energy independent widths (which was experimentally checked for several systems), it is sufficient to measure the excitation functions at one single angle (typically $\theta = 3°$) and normalize them to integrated angular distributions obtained at selected energies. A few examples of some typical excitation functions obtained with the spectrometer are presented in Fig. 6. Beam energy losses in the targets were corrected for by an iterative procedure, taking into account the slopes of the excitation function. At each step, corrected beam energies were obtained by weighting the energies from the previous step by the experimental fusion cross section, and averaging over the energy loss in the target. This process was repeated until self-consistent results were obtained. See Ref. 6 for a more detailed account of this procedure.

As a cross check, we have compared our measurements with previous results obtained with independent methods, when available. In order to compare with the results of Scobel *et al.* [12], we measured the fusion of $^{35}Cl + {}^{58}Ni$ at 100.3 MeV, obtaining a cross section of $\sigma = 44.0 \pm 1.4$ mb, in excellent agreement with the value of $\sigma = 46.9 \pm 4.7$ mb reported in that work for the same energy. We were also able to compare our data [8] for $^{32}S + {}^{58}Ni$ with previous results obtained by Gutbrod *et al.* [13] and the agreement is again excellent, as shown in Fig. 7. In the lower mass region of A around 50, we measured a complete excitation function for $^{32}S + {}^{24}Mg$ in order to compare to the previous data reported by Berkowitz *et al.* [14]. Once again, excellent agreement is observed between the two data sets, as illustrated in Fig. 8, except at the very lowest energies where background events may become important.

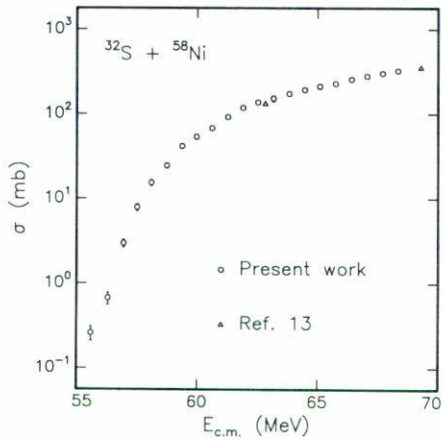

FIGURE 7. Comparison of the fusion excitation function obtained with our spectrometer for $^{32}S+^{58}Ni$ with the data points of Ref. 13.

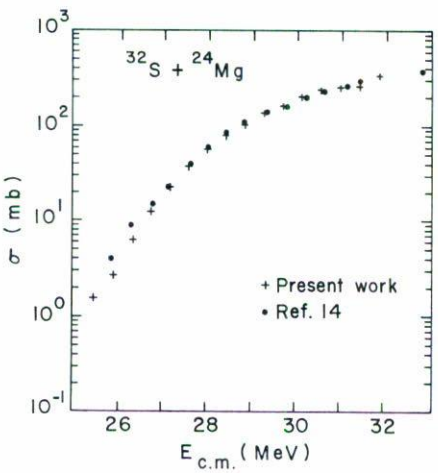

FIGURE 8. Comparison of the fusion excitation functions for $^{32}S+^{24}Mg$ as obtained in this work and in Ref. 14.

5. CONCLUSIONS

The particle detection technique for measuring heavy ion fusion has been illustrated through the detailed description of a recoil-velocity spectrometer especifically designed to detect the evaporation residues in fusion reactions. Unlike the gamma-ray technique, this technique allows the determination of the very low cross sections observed in sub-barrier fusion, where the peak-to-background ratio in the gamma-ray spectra becomes unmeasurably small. Another advantage is the possibility of separating the direct reaction contribution, if any, from the real fusion events by looking at the velocity distribution of the measured residues.

TABLE III. Comparison of the gamma-ray and the particle-detection techniques for measuring heavy-ion fusion reactions.

Feature to be compared	Gamma-ray technique	Particle technique
Experimental device	Very simple	Fairly complex
Data acquisition	Very simple	Fairly complex
Efficiency calibration	Simple	Fomplex
Isotope saparation	Clean	Limited to light systems
Data analysis	Cumbersome	Simple
background elimination	Bad	Good
Detection of g.s. residues	Impossible	No problem
Identification of direct channels	Impossible	Possible
Measurement of low cross sections	Hard	Relatively easy

The major difficulty of separating the evaporation residues from the transmitted beam-like particles is solved in the spectrometer by means of an electrostatic deflector which causes the particles with different electrostatic rigidities to deflect differently. Concerning this, the good performance of the spectrometer can be judged from the beam rejection factor of about 2×10^6, which was experimentally determined for a ^{37}Cl beam at a bombarding energy of 103 MeV on a ^{58}Ni target.

The identification of the residues is achieved with a time-of-flight and energy telescope which gives a mass resolution $\Delta m/m \leq 0.05$. This resolution is good enough to separate the beam-like particles from the evaporation residues for all reactions of interest and even allows, for light systems such as O + C, to resolve the different fusion residues. When the yields observed for the different residues in the ^{17}O + ^{12}C fusion reaction were compared to those predicted by a statistical model calculation, consistent results were found [11].

A Monte Carlo code was written to simulate the performance of the spectrometer. Some important features concerning the transmission efficiency were confirmed by the corresponding calculations, among which are its observed energy and mass insensitivity in the region of $A_{ER} \sim 90$ and $30 \leq E_{ER}(\text{MeV}) \leq 40$; its energy dependence for light systems ($A_{CN} \sim 29$, $E_{ER} \sim 11$ MeV) and/or medium-mass systems but slow ions ($A_{CN} \sim 100$, $E_{ER} \sim 9$ MeV); and its relative flatness as a function of the deflecting voltage for all considered systems.

Finally, a comparative tabulation is presented in Table III, where the advantages and limitations of the gamma-ray technique, described in Ref. 1, and the particle-detection technique here described, are emphasized. It is clear that the comparison made in the first four rows of the Table III favors the gamma-ray technique and in particular the point mentioned in row 4 makes this the best technique for works related with searches for resonances or statistical-model tests, where a clean separation of the different evaporation channels is important. Possible exceptions to this statement arise in the case of light systems, where the same nuclei may be reached either by fusion-evaporation or by direct-reaction channels. Careful observation of rows 4 and 8 of Table III indicates that in this

case the particle-detection technique might give the best results for the mentioned kind of works. We also see that the last 5 rows of the table favor the particle detection technique, and in particular row 9 indicates that this should be the prefered technique for works where low cross sections have to be measured, such as sub-barrier fusion studies.

REFERENCES

1. E.F. Aguilera, *Rev. Mex. Fís.* **43** (1997) 600.
2. E.F. Aguilera, J.J. Vega, E. Martinez, J.J. Kolata, and A. Morsad, *Rev. Mex. Fís.* **35** (1989) 489.
3. F. Pühlhofer, *Nucl. Phys.* **A 280** (1977) 267.
4. J. Gomez del Campo and R.G. Stokstad, ORNL Report No. TM-7295; J. Gomez del Campo, R.G. Stokstad, J.A. Biggerstaff, R.A. Dayras, A.H. Snell, and P.H. Stelson, *Phys. Rev. C* **19** (1979) 2170.
5. V.S. Nikolaev and I.S. Dmitriev, *Phys. Lett.* **A 28** (1968) 277.
6. E.F. Aguilera, J.J. Vega, J.J. Kolata, A. Morsad, R.G. Tighe, and X.J. Kong, *Phys. Rev. C* **41** (1990) 910.
7. J.J. Vega, E.F. Aguilera, G. Murillo, J.J. Kolata, A. Morsad, and X.J. Kong, *Phys. Rev. C* **42** (1990) 947.
8. R.J. Tighe, J.J. Vega, E. Aguilera, G.B. Liu, A. Morsad, J.J. Kolata, S.H. Fricke, H. Esbensen, and S. Landowne, *Phys. Rev. C* **42** (1990) 1530.
9. E.F. Aguilera, J.J. Kolata, and R.J. Tighe, *Phys. Rev. C* **52** (1995) 3103.
10. A. Morsad, J.J. Kolata, R.J. Tighe, X.J. Kong, E.F. Aguilera, and J.J. Vega, *Phys. Rev. C* **41** (1990) 988.
11. R.J. Tighe, J.J. Kolata, M. Belbot, and E.F. Aguilera, *Phys. Rev. C* **47** (1993) 2699.
12. W. Scobel, H.H. Gutbrod, M. Blann, and A. Mignerey, *Phys. Rev. C* **14** (1976) 1808.
13. H.H. Gutbrod, W.G. Winn, and M. Blann, *Nucl. Phys.* **A 213** (1973) 267.
14. G.M. Berkowitz, P. Braun-Munzinger, J.S. Karp, R.H. Freifelder, T.R. Renner, and H.W. Wilschut, *Phys. Rev. C* **28** (1983) 667